Tailoring Li adsorption on graphene

Jian Zhou,[1] Qiang Sun,[2,3,1] Qian Wang,[3,2,1] and Puru Jena[1,*]

[1]*Department of Physics, Virginia Commonwealth University, Richmond, Virgina 23284, USA*

[2]*Department of Materials Science and Engineering, College of Engineering, Peking University, Beijing 100871, China*

[3]*HEDPS, Center for Applied Physics and Technology, Peking University, Beijing 100871, China*

The technological potential of functionalized graphene has recently stimulated considerable interest in the study of the adsorption of metal atoms on graphene. However, a complete understanding of the optimal adsorption pattern of metal atoms on a graphene substrate has not been easy because of atomic relaxations at the interface and the interaction between metal atoms. We present a partial particle swarm optimization technique that allows us to efficiently search for the equilibrium geometries of metal atoms adsorbed on a substrate as a function of adatom concentration. Using Li deposition on graphene as an example we show that, contrary to previous works, Li atoms prefer to *cluster*, forming four-atom islands, irrespective of their concentration. We further show that an external electric field applied vertically to the graphene surface or doping with boron can prevent this clustering, leading to the homogeneous growth of Li.

I. INTRODUCTION

Graphene [1], a two-dimensional (2D) honeycomb lattice of carbon atoms, is probably the most studied system in recent times [2]. The ease with which graphene can be functionalized with hydrogen [3–5], oxygen [6–8], and metal atoms [9–11] has further added a new dimension to its potential for novel applications. Atomic layer deposition (ALD) is an efficient surface-controlled thin-film growth technique that is often used to deposit metal atoms on graphene [12]. In this technique, maximum benefit is achieved if the metal atoms are homogenously dispersed on the substrate. However, due to the extended stable π orbitals of graphene and strong affinity of metal atoms toward each other, achieving uniform ALD of metals on graphene has been experimentally difficult. Metals generally tend to disperse inhomogeneously and cluster to form islands on the graphene sheet [13–15].

First-principles calculation of the optimal adsorption pattern of finite-size metal particles is difficult due to interfacial relaxation and metal-metal interaction. In addition, the energy landscape contains many local minima and finding the global equilibrium geometry of the particle may depend on the choice of the starting configuration. The problem becomes even more complicated when the interaction of the particle with the support is considered as there are many sites where the particle has the freedom to reside. We present an efficient search technique to find the optimal adsorption pattern of metal atoms adsorbed on a substrate. This method is based on the particle swarm optimization (PSO) algorithm developed recently by Ma and his group for searching globally optimal structures of three-dimensional (3D) crystals, 2D sheets, and 0D clusters [16]. By only using chemical component information, these authors have been successful in determining stable configurations of O_4, Li, and ice under high pressure [17–19]. We refer to our search algorithm as *partial* particle swarm optimization (PPSO) method. We demonstrate the

power of this algorithm by focusing on the surface structure of Li-functionalized graphene.

Our choice of Li-decorated graphene sheet [20–23] as a test case is motivated because of its potential in hydrogen storage [24], Li-ion batteries [25,26], and superconducting materials [27–29]. To the best of our knowledge, most of the theoretical works thus far assumed, in analogy with multilayer graphite intercalated compounds (GICs), that the Li atoms are *uniformly* distributed on the graphene surface [24,27–30]. However, due to the inactive delocalized π orbitals of graphene, the diffusion barrier of Li atoms on its surface is small. As a result, the Li atoms tend to move and cluster. Since clustering may adversely affect the performance of Li-decorated graphene, it is not only important to study the distribution patterns of Li on graphene but also to find ways to prevent their clustering. The basic questions we address are as follows. Can we predict the cluster pattern of Li atoms adsorbed on graphene? How sensitive are the properties to the nature of this distribution pattern? Can we find an effective method to tailor this pattern? First-principles calculation of the total energies combined with the PPSO algorithm shows that the Li atoms do not uniformly distribute on the graphene sheet, as assumed in previous calculations, but rather they form four-atom islands in the shape of a rhombus. This pattern is found to persist for different concentrations of Li, namely, LiC_x ($x = 6 - 9$). However, this adsorption pattern can be modulated by either applying an external electric field (E field) or by chemically modifying the graphene substrate. In Sec. II we describe our theoretical method. The results are presented and discussed in Sec. III and conclusions are drawn in Sec. IV.

II. THEORETICAL METHODS

The total energies for a given arrangement of atoms were calculated from first principles using density functional theory (DFT) with the Perdew-Burke-Ernzerhof (PBE) functional for the generalized gradient approximation (GGA) to exchange-correlation potential [31], as implemented in Vienna *Ab initio* Simulation Package (VASP) [32]. The projector augmented plane-wave (PAW) method [33] and a plane-wave basis set

———
*Corresponding author: pjena@vcu.edu

with an energy cutoff of 400 eV were used. Monkhorst-Pack k-point meshes [34] with a grid density of $2\pi \times 0.02$ Å^{-1} were adopted. We used a vacuum space of 15 Å along the z direction in order to prevent interaction between nearest-neighbor images. In order to incorporate van der Waals (vdW) interaction corrections between the Li atoms and the graphene, Grimme's method [35] was employed. Conjugate gradient method was used to optimize the atomic configurations without any symmetric constraints. Convergence criteria for total energy and the force component on each atom were set to be 10^{-4} eV and 0.01 eV/Å, respectively. External electric field was applied using the planar dipole layer method [36]. Dipole interaction corrections were taken into account following the work of Makov and Payne [37].

In the PPSO method, we fix the coordinates of the C atoms in the graphene, while allowing the coordinates of Li atoms to evolve using the PSO algorithm [16]. First, 20 different Li adsorption patterns were randomly generated and then relaxed using the DFT calculations. Each structure (called an individual in the algorithm) is considered as a particle in the search space. The position of each particle x is evolved as

$$x_i^{t+1} = x_i^t + v_i^{t+1}, \tag{1}$$

where t refers to the generation step, i is individual particle index ($i = 1, 2, \ldots, 20$), and v is the velocity. For each individual, we collect the current best (lowest energy) position that has been reached, and denote it as pbest_i^t. The best position of all the particles that have been found is denoted as gbest^t. The new velocity of each particle is written as

$$v_i^{t+1} = \omega v_i^t + c_1 r_1 \left(\text{pbest}_i^t - x_i^t\right) + c_2 r_2 \left(\text{gbest}^t - x_i^t\right), \tag{2}$$

where r_1 and r_2 are random numbers in the range [0,1]. The parameter ω linearly decreases from 0.9 to 0.4 during the iteration. The values of c_1 and c_2 are selected to be 2, which are found to efficiently lead to the global minimum [16].

In order to reduce the constraints imposed by periodicity, we used different size supercells for each Li:C ratio. For the Li:C ratio of 1:6, we used $(2\sqrt{3} \times 2\sqrt{3})R30°$, (6×6), and $(4\sqrt{3} \times 4\sqrt{3})R30°$ supercells to accommodate Li$_4$C$_{24}$, Li$_{12}$C$_{72}$, and Li$_{16}$C$_{96}$, respectively. For the Li:C ratio of 1:7, we used $(2\sqrt{7} \times 2\sqrt{7})R19.0°$ and (7×7) supercells to accommodate Li$_8$C$_{56}$ and Li$_{14}$C$_{98}$, respectively. For the Li:C ratio of 1:8, (4×4), (6×6), $(4\sqrt{3} \times 4\sqrt{3})R30°$, and (8×8) supercells were used to accommodate Li$_4$C$_{32}$, Li$_9$C$_{72}$, Li$_{12}$C$_{96}$, and Li$_{16}$C$_{128}$, respectively. Finally, for the Li:C ratio of 1:9, we applied $(3\sqrt{3} \times 3\sqrt{3})R30°$ and (6×6) supercells which account for Li$_6$C$_{54}$ and Li$_8$Li$_{72}$, respectively. For each supercell, the PPSO search lasted for at least 30 generation loops, and in each loop 20 different structures were optimized. All structures generated in each iteration loop were relaxed at the DFT-GGA level of theory. Eight of the high-energy structures (40%) in each iteration loop were discarded and replaced by random structures for subsequent generation. The remaining 12 structures (60%) are kept and evolved by the PPSO algorithm. In Fig. 1 we plot the binding energies per Li $[E_b = (E_{\text{Li}mCn} - E_{Cn} - mE_{\text{Li}})/m]$ for all the structures obtained during the PPSO search. For each Li:C ratio, we only report the structure with the lowest energy per formula

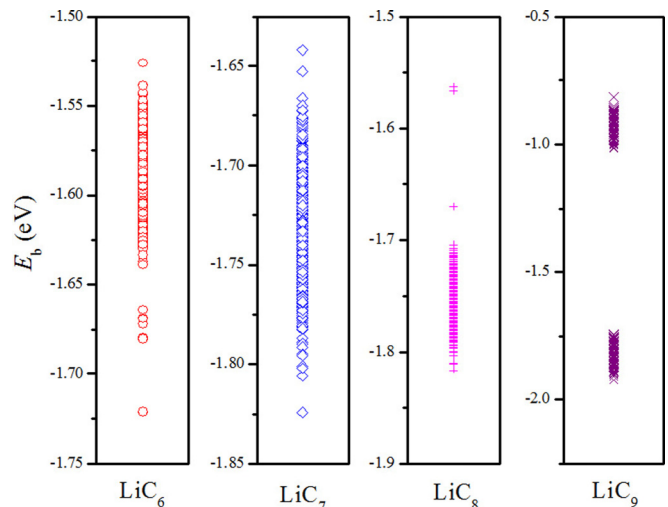FIG. 1. (Color online) Calculated binding energies per Li atom (E_b) of LiC$_x$ ($x = 6 - 9$) obtained during the PPSO search.

unit (E/f.u.). At the end we find that many individuals have converged to the global optimized geometry.

III. RESULTS AND DISCUSSION

We first discuss our results for LiC$_6$ system. The lowest energy structure obtained after our PPSO search is shown in Fig. 2(a). This optimal structure is found in the $(2\sqrt{3} \times 2\sqrt{3})R30°$ supercell (Table I), which contains 24 C and 4 Li atoms. All the Li atoms prefer to reside over hollow sites of the graphene sheet, consistent with previous results [20–25]. However, unlike a uniform distribution pattern (which has a symmetry group of $P6mm$); the four Li atoms form a rhombus structure. Energy calculations show that this structure is more stable than the widely used uniform distribution pattern
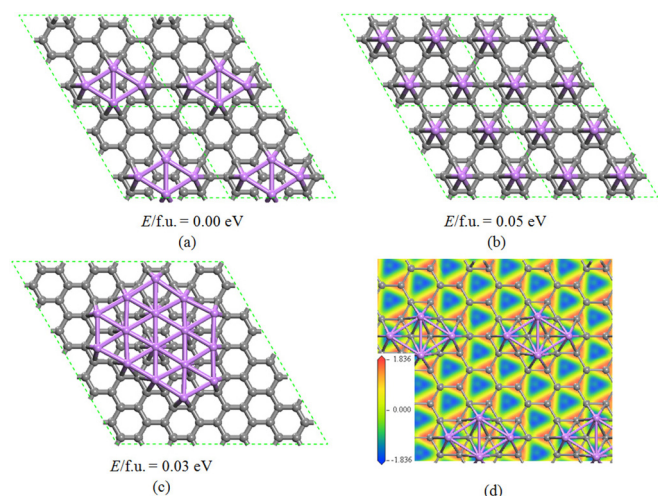

FIG. 2. (Color online) Structures and relative energies of LiC$_6$ with Li atoms forming (a) a Li$_4$ cluster (LiC$_6$-$Cmm2$), (b) uniformly distributed Li (LiC$_6$-$P6mm$), and (c) a Li$_{16}$ cluster. In (d) we show the redistribution of electron density function in 2D slice form (in e/Å^3). Gray and magenta spheres represent C and Li atoms, respectively. Green dashed lines outline simulated supercell.

TABLE I. Supercell type, lattice constant (c), biaxial tensile strain on graphene (ε), average Li-Li bond length ($R_{Li\text{-}Li}$), average charge on Li (Q_{Li}), carrier concentration of graphene sheet (n), and binding energy per Li atom (E_b) in the optimized LiC_6, LiC_7, LiC_8, and LiC_9 structures.

	LiC_6	LiC_7	LiC_8	LiC_9
Supercell	$(2\sqrt{3}\times2\sqrt{3})R30°$	$(2\sqrt{7}\times2\sqrt{7})R19.0°$	(4×4)	(6×6)
c (Å)	8.60	13.14	9.92	14.85
ε (%)	0.9	0.9	0.8	0.6
$R_{Li\text{-}Li}$ (Å)	2.70	2.73	2.73	2.74
Q_{Li} (e)	0.49	0.50	0.49	0.50
n ($\times10^{14}$ cm^{-2})	3.06	2.65	2.31	2.08
E_b (eV)	−1.72	−1.82	−1.82	−1.82

[Fig. 2(b)] by 50 meV per f.u. In the lowest energy structure, the relaxed lattice constant is 8.60 Å, indicating that the substrate graphene has a 0.92% biaxial tensile strain following Li adsorption. The graphene sheet remains almost flat and the distance between the Li and the graphene is 1.93 Å, which is similar to the value in the uniform LiC_6-$P6mm$ system. The average of Li-Li bond length is 2.70 Å, which is a little longer than the equilibrium bond length in its dimer form, namely, 2.67 Å [39]. The structure in Fig. 2(a) belongs to the *Cmm2* space group. Using Bader's charge analysis [40] we find that, on average, each Li atom transfers 0.49 electrons to the graphene substrate, making the graphene n-doped with a carrier concentration of 3.06×10^{14} cm^{-2}. The injected electrons disperse almost uniformly on graphene with the C atoms under Li carrying slightly more charge than the other C atoms due to stronger electrostatic attraction from the positively charged Li. The redistributed electron density $\Delta\rho(=\rho_{Li4C24} - \rho_{Li4} - \rho_{C24})$ is plotted in Fig. 2(d). We see that each C atom receives almost the same amount of charge. The cohesive energy $E_{coh}(=E_{Li4} + E_{C24} - E_{Li4C24})$ between the Li_4 cluster and the graphene is calculated to be 1.53 eV, the positive value indicating exothermic reaction following Li adsorption.

In order to see if the use of a larger supercell for the same Li:C ratio of 1:6 can lead to the formation of larger Li clusters, we used a $(4\sqrt{3}\times4\sqrt{3})R30°$ supercell that contains 16 Li and 96 C atoms with all the 16 atoms forming a cluster. We studied different kinds of Li_{16} clusters, and the structure with the lowest energy is shown in Fig. 1(c). While this pattern is energetically lower than the uniform LiC_6-$P6mm$ pattern, it is higher in energy than the LiC_6-$Cmm2$ pattern by 30 meV per f.u. We have also compared Li_4 with Li_3 and Li_5 clusters on graphene and found that the Li_4 cluster is the most stable pattern [38]. There are two competing mechanisms that are

responsible for the clustering of Li, an attractive interaction resulting from Li-Li bond formation and a repulsive interaction between Li atoms as each carries a positive charge due to charge transfer from Li to graphene. It is the balance between these competing interactions that limits the size of the Li island. We further note that Li_4 clusters combined with four electrons contributed by the C atoms constitute an eight-electron system that corresponds to shell closing and hence provides stability.

Since the uniform distribution of Li on a single-layer graphene (LiC_6-$P6mm$ pattern) was initially taken from the experimental multilayer graphite intercalation compounds (GIC), we examined if such Li_4 clustering is also favored in the GIC. We used a two-layer graphene and intercalated one layer of Li as an example [38]. Simulation of the corresponding supercell (C_{24}-Li_4-C_{24}) showed that Li atoms distribute uniformly, in agreement with experiment. The reason why Li atoms do not cluster when intercalated between two graphene layers is that the net charge on the Li atom increases due to increasing charge transfer. Hence, the Li-Li repulsion overcomes the energy that can be otherwise gained from Li-Li bond formation. However, if we add four more Li atoms on the surface of C_{24}-Li_4-C_{24}, forming C_{24}-Li_4-C_{24}-Li_4, the four Li atoms on the surface again cluster [38]. These results show that only when Li atoms are exposed on the graphene surface do they favor the formation of Li_4 clusters over uniform distribution.

Similar clustering has also been found when Li:C ratio increases. We have used the PPSO search algorithm to study LiC_7, LiC_8, and LiC_9 systems. The optimal LiC_7 found in the $(2\sqrt{7} \times 2\sqrt{7})R19.0°$ supercell [Fig. 3(a)], which contains 8 Li and 56 C atoms. The lattice constant is optimized to be 13.14 Å, showing a 0.9% tensile strain in the graphene layer (Table I). The optimal Li adsorption pattern is again when four Li atoms cluster together, forming two Li_4 cluster islands. The relative positions of the two islands have small effect on the total energy of the system, but they do not favor to furthermore cluster together (i.e., forming a Li_8 cluster). The average relaxed Li-Li bond length is 2.73 Å, and each Li transfers 0.50 electrons to the graphene sheet. In this case, the substrate graphene is n-doped with an electron concentration of 2.65×10^{14} cm^{-2}. For the Li:C ratio of 1:8 (LiC_8), the optimal structure is found in the (4×4) supercell [Fig. 3(b)], containing 4 Li and 32 C atoms. As before, the 4 Li atoms form a rhombus cluster and the graphene is stretched (0.8%) a little. Compared with Li uniform distribution pattern, this structure is energetically lower by 140 meV per f.u. [38]. Each Li gives 0.49 electrons to the graphene sheet, and the electron concentration of graphene is 2.31×10^{14} cm^{-2}. For the LiC_9, we again find that the optimal structure of 8 Li atoms forming two Li_4 cluster islands in a (6×6) supercell [Fig. 3(c)]. This
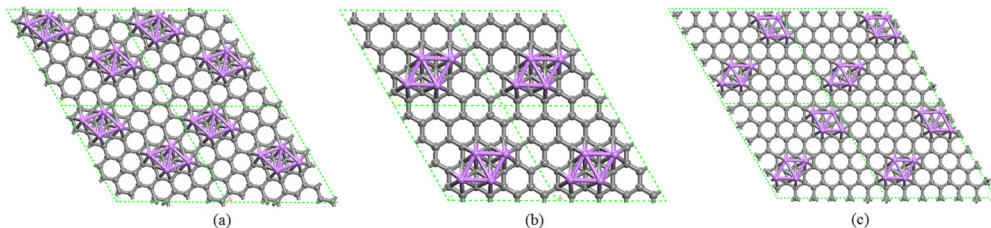

FIG. 3. (Color online) Geometric structure of optimal (a) LiC_7, (b) LiC_8, and (c) LiC_9.

TABLE II. Different exchange-correlation functional and vdW correction effects on $\Delta E/$f.u.

$\Delta E/$f.u. (in eV)	PBE with vdW	PW91 with vdW	PBE w/o vdW	PW91 w/o vdW
LiC_6	−0.05	−0.06	−0.04	−0.05
LiC_8	−0.14	−0.15	−0.13	−0.15
LiC_9	−0.17	−0.18	−0.16	−0.18

is energetically lower by 170 meV per f.u. than the uniformly distributed Li adsorption pattern [38]. The graphene substrate is 0.6% stretched, and the electron concentration is 2.08×10^{14} cm^{-2}. We note that as the Li concentration decreases, the tensile strain and the carrier concentration of the graphene are correspondingly reduced. We should stress that for other types of supercells we mentioned above, the formation of a Li_4 cluster is also preferred, suggesting that our proposed Li decoration pattern is reliable and universal.

To see if our results are sensitive to the choice of exchange-correlation functionals, we repeated our calculation using Perdew-Wang (PW91) functional [41]. The calculated energy difference $\Delta E/$f.u.$(=E_{cluster}/$f.u.$-E_{uniform}/$f.u.$)$ between the clustering and uniform distribution patterns are given in Table II. For the LiC_6, the PW91 functional yields $\Delta E/$f.u.$=-0.06$ eV, which is consistent with the PBE result. We also removed the vdW interactions to consider its effects. We see that $\Delta E/$f.u. becomes smaller, but the stability of the Li_4 clustering pattern is still favored. For the LiC_8 and LiC_9, similar effects are obtained. These calculations show

that our results are not sensitive to either exchange-correlation functionals or vdW interaction. Hence, we mainly focus on the PBE-vdW results in this work.

We next study the effect of Li clustering on the electronic properties of functionalized graphene and compared it to the case when Li atoms distribute uniformly. In Figs. 4(a)–4(d) we plot the energy band structures and projected density of states (PDOS) of LiC_6, LiC_7, LiC_8, and LiC_9. All systems are metallic. In Fig. 4(e)–4(h), we plot the momentum space folding of the simulating supercells. We clearly see that the graphene Dirac point can be folded to the Γ point of the $(2\sqrt{3} \times 2\sqrt{3})R30°$ and (6×6) supercells, while it remains at the K point of the $(2\sqrt{7} \times 2\sqrt{7})R19.0°$ and (4×4) supercells. The Dirac points of the graphene are below the Fermi energy by about 1.3 eV, showing that the graphene substrate is n-doped. At the Dirac point, the band opens a small gap upon Li adsorption. As the GGA-PBE level of theory generally underestimates the band gap, we further verified the metallic feature by using a more accurate screened Coulomb hybrid density functional HSE06 [42,43]. The corresponding results
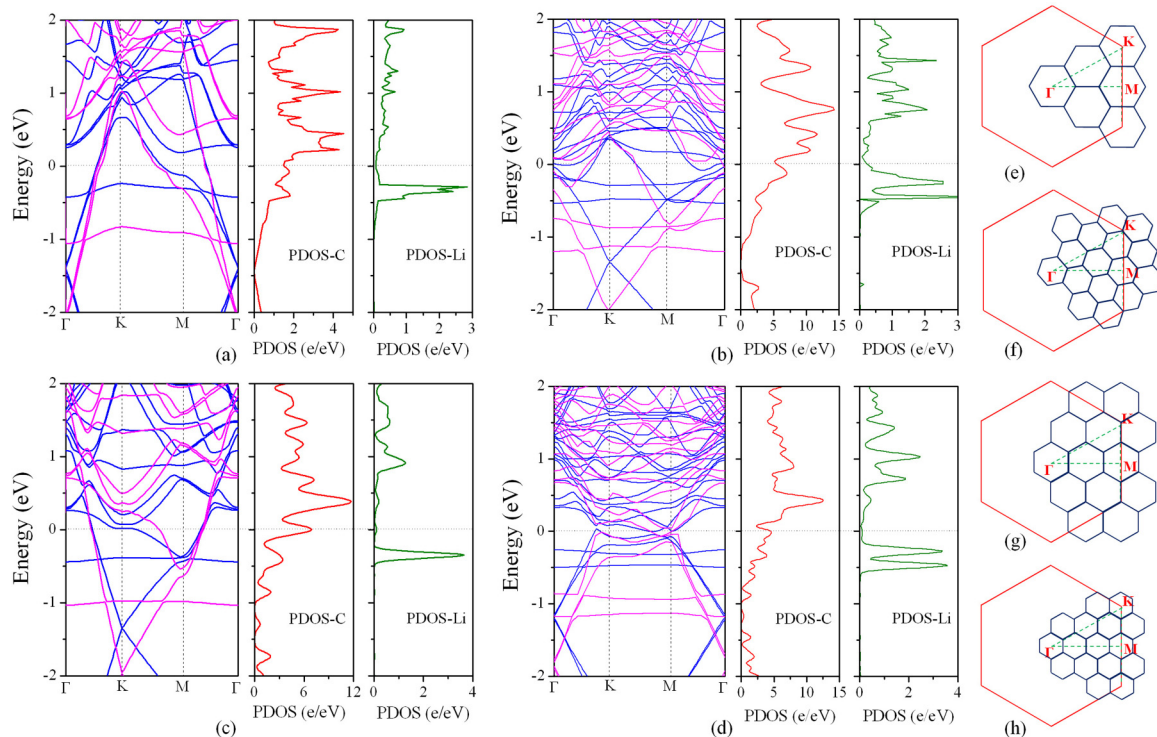

FIG. 4. (Color online) Band structure and PDOS of (a) LiC_6, (b) LiC_7, (c) LiC_8, and (d) LiC_9. Blue and magenta curves in the band structure plots represent results obtained from GGA-PBE and hybrid functional HSE06, respectively. The PDOS curves are computed using the GGA-PBE functional. Momentum space folding of the simulating supercells for (e) LiC_6, (f) LiC_7, (g) LiC_8, and (h) LiC_9 are also shown. Red hexagon represents the first Brillouin zone of the graphene unit cell, while dark blue hexagons are the first Brillouin zone of the simulated supercell.
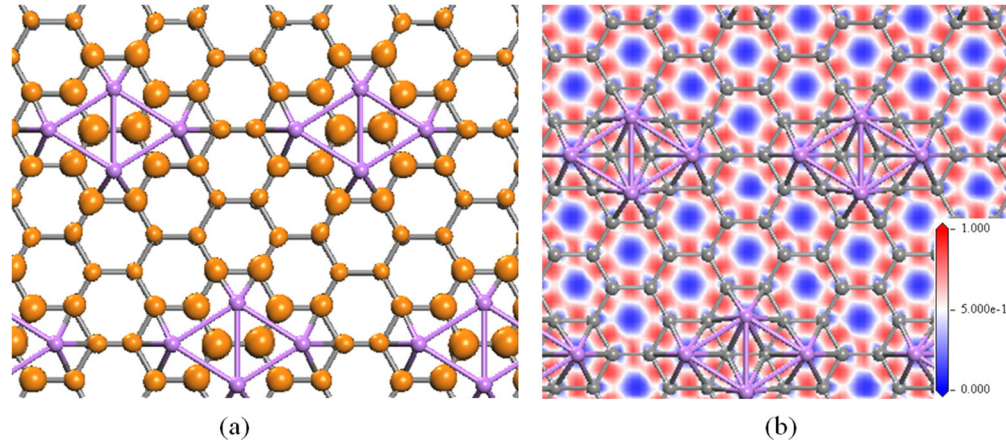
(a)

(b)

FIG. 5. (Color online) (a) Charge density isosurface (0.01 $e/\text{Å}^3$) of the partially occupied bands and (b) 2D slice of ELF of LiC_6.

are given in Fig. 4. Note that the HSE06 only results in a shift of band energies compared with the GGA-PBE level, but the metallic feature is retained. Thus, in the PDOS plots we only use the results from PBE-functional.

We now provide an in-depth analysis of the origin of metallicity by focusing on LiC_6-*Cmm2* as an example [Fig. 4(a)]. From the PDOS plot we see that the metallic bands across the Fermi level are mainly contributed by the C electrons of the graphene sheet while Li atoms have marginal contribution. The main peak due to Li occurs at around -0.4 eV below the Fermi energy. The corresponding band is less dispersed, indicating spatially localized states. This feature is consistent with the weak interaction between different isolated Li_4 cluster islands. We also plot the band decomposed charge density of all metallic bands at the Fermi level in Fig. 5(a). We again find that the metallic bands are contributed only by the C-p_z orbital of the graphene sheet. Note that this feature is in marked contrast with the results in LiC_6-*P6mm*, where the Li atoms also contribute to the metallic bands [23]. Since the electron localization function (ELF) [44] is widely used to describe the extent of spatial distribution of electrons in molecules [45] and in crystals [46], we calculated the ELF of LiC_6-*Cmm2*. The results are plotted in Fig. 5(b). The definition of ELF is based on the jellium homogeneous electron gas and its value is renormalized between 0.0 and 1.0. The values of 0.0, 0.5, and 1.0 represent very low charge density, fully delocalized, and fully localized electrons, respectively. We see that the delocalized electrons are within the region of the C atoms. This confirms that the metallicity arises from the graphene substrate. Similar phenomena are also found in the LiC_7, LiC_8, and LiC_9 systems [38]. We should emphasize that even though the relative positions and directions of the Li_4 cluster island may change, the main conclusions stated above are robust.

We now assess the effect of Li clustering on possible applications of the Li-functionalized graphene, such as Li-ion batteries, hydrogen storage material, and superconductor, considered earlier [20–25]. We recall that in all these applications Li atoms were assumed to distribute uniformly. As the Li atoms form stable Li_4 clusters when deposited on graphene, it is unlikely that one Li atom can move freely on the graphene sheet without being obstructed by other Li atoms. Hence, clustering may decrease the mobility of Li and hence battery performance. As for hydrogen storage

materials, it is well known that the clustering of metal atoms will reduce both the binding energy of hydrogen molecules as well as the gravimetric density [47]. Thus, it is unlikely that Li-functionalized pure graphene sheet can be an ideal Li-ion battery or hydrogen storage material. As for possible superconductivity, it has been proposed that LiC_6-*P6mm* can be a superconductor with critical temperature $T_c = 8.1$ K [23], because the delocalized Li bands cross the Fermi level to a high degree. However, in the LiC_6-*Cmm2*, the Li bands are localized and bounded below the Fermi level. This suggests that the electron-phonon coupling may be weak. Another possible strategy to make graphene superconducting is by external electron doping. Theoretical works have shown that highly doped graphene sheet (up to van-Hove singularity point) can exhibit a $d + id$ chiral superconducting state [48], but our Bader's charge analysis shows that the doping here is small. At intermediate doping level, Si *et al.* [49] have developed an empirical model and suggested that the graphene sheet can become superconducting when biaxial tensile strain and electron doping coexist. However, according to their model, the possible T_c of the LiC_6-*Cmm2* is still very low (<0.1 K), even under biaxial strain [38]. Therefore, we believe that Li-decorated graphene will not have much merit as a superconductor.

The only way Li-functionalized graphene can be useful for applications in hydrogen storage, Li-ion batteries, and superconductivity is to ensure that Li atoms are deposited *uniformly*. We find that although the uniform distribution of Li on graphene is dynamically stable [23], it cannot be retained even below 50 K [38]. Hence, we looked for alternative methods to realize it experimentally. As discussed previously, Li clustering results from two competing interactions: energy gain due to Li-Li bond formation and energy cost to overcome the repulsive interaction between two positively charged Li atoms. Our hypothesis is that clustering can be prevented if the positive charge on the Li atom is increased. Taking LiC_6 as an example, we apply a gate E field to enhance charge transfer between the Li and graphene. As shown in Fig. 6, when an E field is applied, Li atoms transfer electrons and are more positively charged. As Q_{Li} increases, energy difference between the LiC_6-*P6mm* and LiC_6-*Cmm2* is decreased. When E field reaches a value of 1.0 V/Å, the charge, Q_{Li} on the Li atom is 0.56 and the two patterns are energetically degenerate.
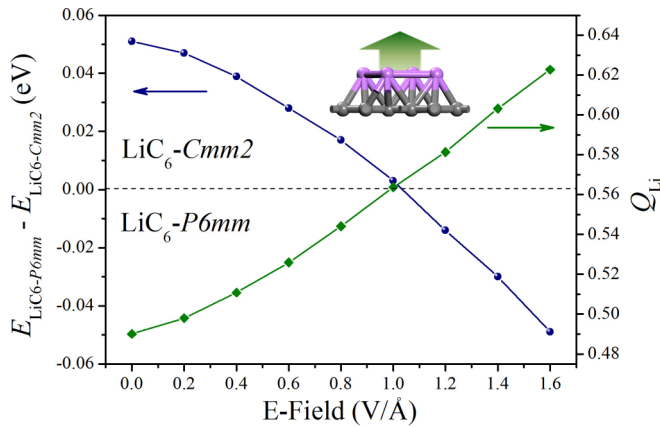
FIG. 6. (Color online) Relative energies between the LiC_6-*P6mm* and LiC_6-*Cmm2* per f.u. and average charges on each Li with respect to magnitude of the E field. The inset arrow shows the direction of the E field.

Once the E field crosses this critical value, the LiC_6-*P6mm* pattern with uniformly distributed Li becomes *more stable* than the LiC_6-*Cmm2* pattern where Li atoms cluster, showing that an E field can be an effective way to promote homogeneous film growth of Li on a graphene sheet. This can be retained under finite temperature of at least up to 100 K [38]. Such method is also verified in the LiC_8 system [38]. Note that Li atoms do not cluster on C_{60} surface [46], which has a higher curvature than that of graphene. Hence, we can infer that uniform deposition is more favorable on a curved surface, such as on thin carbon nanotubes.

Since large positive charge on Li can prevent these atoms from clustering, we have considered another possibility. We note that for a Li atom to transfer a larger amount of charge, the substrate has to be more electronegative. This can be achieved by doping graphene with B atoms. Since a B atom is trivalent and a C atom is tetravalent, replacing a C atom with B would allow Li atom to more easily transfer its electron to B. Thus, the Li atom can be more cationic and hence two Li atoms would experience increasing electrostatic repulsion. We note that this was already shown to be the case in B-doped C_{60} fullerene and carbon nanotubes [50,51]. To study this possibility for graphene we consider experimentally synthesized BC_3 sheet [52] as an example. Two concentrations of Li have been considered, namely, $n_{Li}:(n_C + n_B) = 1:6$ ($Li_2B_3C_9$) and 1:8 (LiB_2C_6). After our PPSO search, we find that the optimal deposition pattern in both concentrations becomes *uniform* (Fig. 7). By examining the charge distribution, the Li atom carries 0.88 (0.87) electrons in the $Li_2B_3C_9$ (LiB_2C_6) case, which is much larger than that in pure graphene. This is consistent with the mechanism we proposed previously. The band structures and PDOS [38] show that both of these systems are metallic. In the $Li_2B_3C_9$, we see an obvious contribution of Li to the metallic bands, which suggests this may be superconducting [23].

IV. CONCLUSIONS

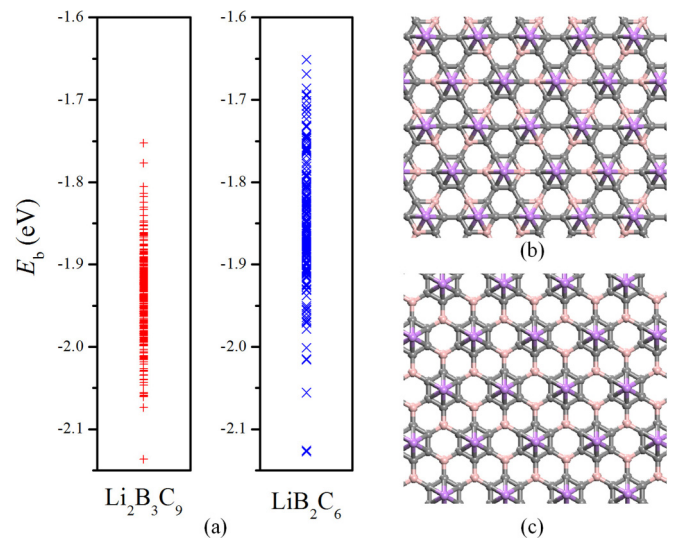In summary, we have applied the PPSO algorithm to search the optimal structure of metal atoms supported on a

FIG. 7. (Color online) (a) The calculated binding energy (E_b) per Li atom of $Li_2B_3C_9$ and LiB_2C_6 obtained during the PPSO search. The ground-state geometry of (b) $Li_2B_3C_9$ and (c) LiB_2C_6.

substrate. This method applied to Li atoms supported on a graphene substrate shows that, contrary to earlier assumptions, Li atoms cluster to form Li_4 cluster islands, irrespective of their concentration. This indicates that the ALD of Li on graphene would lead to inhomogeneous growth. This clustering is driven by two competing mechanisms: a repulsive interaction between Li atoms brought about by charge transfer from Li to graphene (this leads to uniform distribution) and an attractive interaction due to Li-Li bond formation (this favors clustering). We show that either an external electric field applied perpendicular to the graphene substrate or B doping can tilt the balance in favor of *uniform* distribution due to increased charge transfer; hence restoring the promise of Li-functionalized graphene for applications. Since Li has small cohesive energy in its bulk form, most other metals can also have such a clustering problem on graphene. Both our PPSO algorithm and the use of an electric field as well as B doping in modulating the distribution of adatoms on surfaces provide new opportunities for designing functionalized surfaces for targeted applications and for achieving uniform ALD on graphene sheet.

[1] K. S. Novoselov, A. K. Geim, S. V. Morozov, D. Jiang, Y. Zhang, S. V. Dubonos, I. V. Grigorieva, and A. A. Filrsov, Science **306**, 666 (2004).

[2] A. K. Geim, Science **324**, 1530 (2009).

[3] D. C. Elias, R. R. Nair, T. M. G. Mohiuddin, S. V. Morozov, P. Blake, M. P. Halsall, A. C. Ferrari, D. W. Boukhvalov, M. I. Katsnelson, A. K. Geim, and K. S. Novoselov, Science **323**, 610 (2009).

[4] J. O. Sofo, A. S. Chaudhari, and G. D. Barber, Phys. Rev. B **75**, 153401 (2007).

[5] J. Zhou, Q. Wang, Q. Sun, X. S. Chen, Y. Kawazoe, and P. Jena, Nano Lett. **9**, 3867 (2009).

[6] M. Topsakal and S. Ciraci, Phys. Rev. B **86**, 205402 (2012).

[7] B. Huang, H. Xiang, Q. Xu, and S.-H. Wei, Phys. Rev. Lett. **110**, 085501 (2013).

[8] J.-A. Yan and M. Y. Chou, Phys. Rev. B **82**, 125403 (2010).

[9] T. Eelbo, M. Wasniowska, P. Thakur, M. Gyamfi, B. Sachs, T. O. Wehling, S. Forti, U. Starke, C. Tieg, A. I. Lichtenstein, and R. Wiesendanger, Phys. Rev. Lett. **110**, 136804 (2013).

[10] F. Donati, L. Gragnaniello, A. Cavallin, F. D. Natterer, Q. Dubout, M. Pivetta, F. Patthey, J. Dreiser, C. Piamonteze, S. Rusponi, and H. Brune, Phys. Rev. Lett. **113**, 177201 (2014).

[11] J.-H. Parq, J. Yu, Y.-K. Kwon, and G. Kim, Phys. Rev. B **82**, 193406 (2010).

[12] S. M. George, Chem. Rev. **110**, 111 (2010).

[13] X. Liu, C. Z. Wang, Y. X. Yao, W. C. Lu, M. Hupalo, M. C. Tringides, and K. M. Ho, Phys. Rev. B **83**, 235411 (2011).

[14] X. Liu, M. Hupalo, C.-Z. Wang, W.-C. Lu, P. A. Thiel, K.-M. Ho, and M. C. Tringides, Phys. Rev. B **86**, 081414(R) (2012).

[15] W. Li, Y. He, L. Wang, G. Ding, Z.-Q. Zhang, R. W. Lortz, P. Sheng, and N. Wang, Phys. Rev. B **84**, 045431 (2011).

[16] Y. Wang, J. Lv, L. Zhu, and Y. Ma, Phys. Rev. B **82**, 094116 (2010).

[17] L. Zhu, Z. Wang, Y. Wang, G. Zou, H.-k. Mao, and Y. Ma, Proc. Natl. Acad. Sci. USA **109**, 751 (2012).

[18] Y. Wang, H. Liu, J. Lv, L. Zhu, H. Wang, and Y. Ma, Nat. Commun. **2**, 563 (2011)

[19] J. Lv, Y. Wang, L. Zhu, and Y. Ma, Phys. Rev. Lett. **106**, 015503 (2011).

[20] E. J. Yoo, J. Kim, E. Hosono, H.-s. Zhou, T. Kudo, and I. Honma, Nano Lett. **8**, 2277 (2008).

[21] K.-H. Jin, S.-M. Choi, and S.-H. Jhi, Phys. Rev. B **82**, 033414 (2010).

[22] M. A. Romero, A. Iglesias-García, and E. C. Goldberg, Phys. Rev. B **83**, 125411 (2011).

[23] K. T. Chan, J. B. Neaton, and M. L. Cohen, Phys. Rev. B **77**, 235430 (2008).

[24] C. Ataca, E. Aktuerk, S. Ciraci, and H. Ustunel, Appl. Phys. Lett. **93**, 043123 (2008).

[25] J. Langer, V. Epp, P. Heitjans, F. A. Mautner, and M. Wilkening, Phys. Rev. B **88**, 094304 (2013).

[26] E. Lee and K. A. Persson, Nano Lett. **12**, 4624 (2012).

[27] G. Profeta, M. Calandra, and F. Mauri, Nat. Phys. **8**, 131 (2012).

[28] T. P. Kaloni1, A. V. Balatsky, and U. Schwingenschlogl, Europhys. Lett. **104**, 47013 (2013).

[29] B. Uchoa and A. H. Castro Neto, Phys. Rev. Lett. **98**, 146801 (2007).

[30] M. Khantha, N. A. Cordero, L. M. Molina, J. A. Alonso, and L. A. Girifalco, Phys. Rev. B **70**, 125422 (2004).

[31] J. P. Perdew, K. Burke, and M. Ernzerhof, Phys. Rev. Lett. **77**, 3865 (1996).

[32] G. Kresse and J. Furthmuller, Phys. Rev. B **54**, 11169 (1996).

[33] P. E. Blöchl, Phys. Rev. B **50**, 17953 (1994).

[34] H. J. Monkhorst and J. D. Pack, Phys. Rev. B **13**, 5188 (1976).

[35] S. Grimme, J. Comput. Chem. **27**, 1787 (2006).

[36] J. Neugebauer and M. Scheffler, Phys. Rev. B **46**, 16067 (1992).

[37] G. Makov and M. C. Payne, Phys. Rev. B **51**, 4014 (1995).

[38] See Supplemental Material at http://link.aps.org/supplemental/ 10.1103/PhysRevB.90.205427 for relative energies between Li_3, Li_4, and Li_5 clusters on graphene, relative energies of different patterns of Li intercalated inside two-layer graphene, relative energies between Li clusters and uniform distribution for LiC_8 and LiC_9, band decomposed charge density of LiC_6, ELFs for LiC_6, LiC_7, LiC_8, and LiC_9, strain-induced charge transfer between Li_4 cluster and the graphene, molecular dynamics simulations for LiC_6-*P6mm* with and without E field, E-field effects on LiC_8 structure, as well as band structures of Li on BC_3.

[39] K. P. Huber and G. Herzberg, *Molecular Spectra and Molecular Structure. IV. Constants of Diatomic Molecules* (Van Nostrand Reinhold, New York, 1979).

[40] W. Tang, E. Sanville, and G. Henkelman, J. Phys.: Condens. Matter **21**, 084204 (2009).

[41] Y. Wang and J. P. Perdew, Phys. Rev. B **44**, 13298 (1991).

[42] J. Heyd, G. E. Scuseria, and M. Ernzerhof, J. Chem. Phys. **118**, 8207 (2003).

[43] J. Heyd, G. E. Scuseria, and M. Ernzerhof, J. Chem. Phys. **124**, 219906 (2006).

[44] A. D. Becke and K. E. Edgecombe, J. Chem. Phys. **92**, 5397 (1990).

[45] B. Silvi and A. Savin, Nature (London) **371**, 683 (1994).

[46] A. Savin, O. Jepsen, J. Flad, O. K. Andersen, H. Preuss, and H. G. von Schnering, Angew. Chem. Int. Ed. **31**, 187 (1992).

[47] Q. Sun, Q. Wang, P. Jena, and Y. Kawazoe, J. Am. Chem. Soc. **127**, 14582 (2005).

[48] R. Nandkishore, L. S. Levitov, and A.V. Chubukov, Nat. Phys. **8**, 158 (2012).

[49] C. Si, Z. Liu, W. Duan, and F. Liu, Phys. Rev. Lett. **111**, 196802 (2013).

[50] Q. Sun, Q. Wang, and P. Jena, Appl. Phys. Lett. **94**, 013111 (2009).

[51] J. Zhou, Q. Wang, Q. Sun, and P. Jena, J. Phys. Chem. C **115**, 6136 (2011).

[52] H. Tanaka, Y. Kawamata, H. Simizu, T. Fujita, H. Yanagisawa, S. Otani, and C. Oshima, Solid State Commun. **136**, 22 (2005).